Int. J. Electrochem. Sci., 14 **(2019)** 2683 – 2692, doi: 10.20964/2019.03.24

International Journal of
ELECTROCHEMICAL
SCIENCE
www.electrochemsci.org

Corrosion behavior of AISI321 stainless steel in an ethylene glycol-water solution

Xiaoguang Zhang[1], Xiang Liu[2], Wenping Dong[2], Endian Fan[3], Ziheng Bai[3], Gengkai Hu[1], Pan Yi[3], Kui Xiao[3], Yunhua Huang[3,]*

[1] School of Aerospace Engineering，Beijing Institute of Technology, No.5 South Zhongguancun Street, Beijing 100081, China
[2] National key laboratory of human factors engineering, China astronaut research and training center, Beijing 100094, China
[3] Institute of Advanced Materials and Technology, University of Science and Technology Beijing, Beijing 100083, China.
[*]E-mail: huangyh@mater.ustb.edu.cn

Received: 19 July 2018 / *Accepted:* 12 January 2019 / *Published:* 7 February2019

The electrochemical corrosion behaviors of AISI321 stainless steel in a 36% ethylene glycol-water solution are investigated by electrochemical impedance spectroscopy, Mott-Schottky analysis, electrochemical atomic force microscopy and X-ray photoelectron spectroscopy. The results indicated that the calculated donor density increased, as a result of an increasing passive film formation potential, suggesting that the passive film formed at high potential provided much better protection performance. The n-type semiconductor behavior was observed in the potential range from -0.15 to 0.45 V (vs. SCE), however p-type semiconductor behavior was observed in the potential range from 0.45 to 0.75 V, and the carrier density decreased with the increasing potential during the passivation.

Keywords: AISI321 stainless steel; Corrosion; Mott-Schottky analysis; EIS; EC-AFM

1. INTRODUCTION

Stainless steel (SS), found in four main types (ferritic, austenitic, martensitic and duplex), is widely applied in all industries and applications from daily household products to heavy machinery to sophisticated electronic equipment in aerospace industries [1-4]. It is noteworthy that the SS aerospace materials in actual service conditions are usually used in circulating water cooling systems, and thus, some corrosion problems have been observed due to the coolant solutions use in the system such as an ethylene glycol-water aqueous environment [5, 6].

The effect of the ethylene glycol-water solution on corrosion processes is related to the concentration ratio between ethylene glycol and water and the ions present in circulation systems that are dissolved in the coolant solution. Previous research found that in the presence of NO_2^- nitrates, the corrosion rate of the AISI 4130 steel in the glycol-water solution decreased due to the competitive adsorption effect between the NO_2^- and aggressive ions in the solution [7]. However, this inhibition efficiency decreased as the concentration of ethylene glycol increased [8]. In addition to the ions such as NO_2^-, NO_3^- and CrO_4^{2-}, an inhibition effect of the ethylendiamine organic compound was also observed [9, 10]. Simultaneously, the phenomenon of passivation was observed in an ethylene glycol-water solution in the presence of molybdate [11]. Furthermore, the temperature may influence the corrosion processes of metal materials soaked in an ethylene glycol-water solution. For example, Chen investigated the influence of temperature on an aluminum alloy and found that the corrosion rate was increased with increasing temperature [12].

Typically, the excellent corrosion resistance property of stainless steel mainly comes from its passivation and semiconductor behaviors [13, 14]. Although previous studies have revealed the adsorption mechanisms of metal surfaces with ions or organic compound present in ethylene glycol-water, the semiconductor behavior and structural changes of the passive films that are related to the ethylene glycol-water solution still remain poorly understood. Hence, we investigated and elucidated the corrosion behavior of the AISI 321 stainless steel in a 36% ethylene glycol-water solution. Series of electrochemical measurements including polarization curves, electrochemical impedance spectroscopy (EIS) was used. And relevant surface analysis techniques, including in situ electrochemical atomic force microscopy (EC-AFM) and X-ray photoelectron spectroscopy (XPS) were implemented to determine the corrosion behavior of the AISI321.

2. EXPERIMENTS

2.1. Experimental material

The specimens were cut into square pieces with dimensions of 10 mm×10 mm. And the composition is given in Table 1.

Table 1 Chemical composition of the investigated steel (wt%).

Elements	C	Si	Mn	P	S	Cr	Mo	Ni	Cu	Ti	Fe
Weight-%	0.1115	0.676	1.335	0.0322	0.0276	17.605	0.274	9.33	0.2295	0.3015	Balance

The micro-structure were observed by a ZEISS Axio Scope A1 optical microscopy. As shown in Fig. 1, the typical microstructure was austenite.

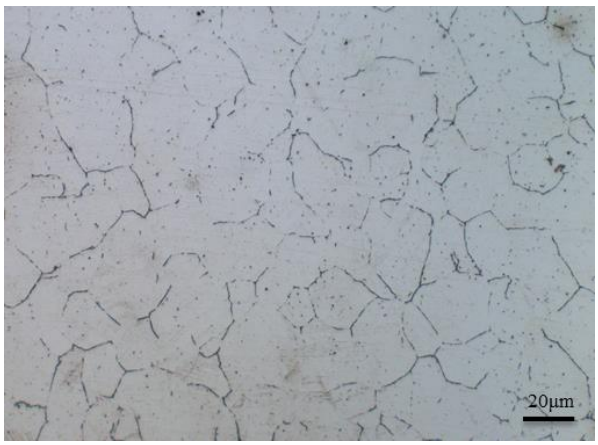

Figure 1. Metallography of AISI321 stainless steel.

2.2. Experimental procedures

The specimens for series of electrochemical tests were welded with copper conductor and then were coated with an epoxy resin. The testing area dimensions were 10 mm × 10 mm and polished to 1 μm pastes. The concentration of 36% ethylene glycol-water was chosen as the testing solution because this concentration is usual in the fields of spaceflight. A VersaSTAT 3F was used for electrochemical test, and all electrochemical tests were conducted in 36% ethylene glycol-water (36 mL ethylene glycol+64 mL deionized water, v:v). A platinum plate was used as the counter electrode (CE), a saturated calomel electrode (SCE) were chosen as the reference electrode (RE). The sample was pretreated cathodically at -1.0 V for 10 minutes before all electrochemical tests to wipe off the air-formed oxidation films [1, 16, 17]. The scanning rate of the potentiodynamic polarization curve was 0.2 $mV\cdot s^{-1}$, from -0.3 to 1.8 V (vs. OCP)

The formation potential 200, 400 and 600 mV of the passive film was chosen in the polarization experiment. Films were formed at each potential for 4 h to ensure that the whole system was in the steady state. Then, the protection performance of the passive film on the substrate was evaluated by EIS experiments. During the EIS measurements, the frequency was from 100 kHz to 10 mHz with a perturbation of 10 mV. And the Mott-Schottky plots were obtaineded by sweeping the potential in the negative direction from 0.75 to 0.15 V, with a frequency response of 1 kHz and a scanning rate of 20 $mV\cdot s^{-1}$. The morphology of the passive film was observed using in situ EC-AFM (Bruker multiMode 8.0). The detailed information concerning the setup and methods used for surface morphology observation are provided in the literature [18]. The chemical composition of the passive films was analyzed by a Thermo ESCALAB 250Xi XPS.

3. RESULTS AND DISCUSSION

3.1. Polarization measurements

The potentiodynamic polarization curve of AISI321 in the testing solution is shown in Fig. 2,

which shows that the corrosion potential of this stainless steel is approximately -253.4 mV. Relevant fitting results and parameters of the polarization measurements are shown in Table 2. It can be concluded that the value of corrosion current density I_{corr} is low and equal to only 83.8 nA. The anodic Tafel slope β_a is larger than that of cathodic β_c, and therefore, the electrochemical behavior is controlled by anodic reaction. Beyond the Tafel region, the AISI321 performs a wide range of passivation behavior. According to the anodic region, the active, passive and transpassive regions is clearly observed. Among them, the active region is located between -0.25 and -0.15 V, the passive region ranges is from -0.15 to 0.75 V, and the transpassive region is above 0.75 V_{SCE}.

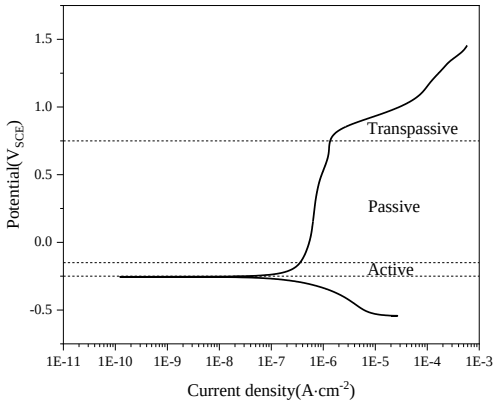

Figure 2. The potentiodynamic polarization curve of AISI321 in 36% ethylene glycol-water solution at a scanning rate of 0.2 mV· s^{-1}.

Table 2 The parameters fitted from the polarization curve in Fig. 2

E_{corr} (mV_{SCE})	I_{corr} (nA)	β_c (mV_{SCE})	β_a (mV_{SCE})
-253.4	83.8	70.1	260.7

3.2. EIS measurements

Based on the polarization curve, three different film formation potentials (200, 400 and 600 mV) during the passive region were selected for potentiostatic film formation. The specimen was polarized at each film formation potential for 4 h before EIS test. Subsequently, the protection performance of the passive film was studied using EIS measurements. The electrochemical system should be a linear and stable system so that valid EIS can be obtained [15, 19-22].

The Nyquist and Bode diagrams are shown in Fig. 3. The Bode diagram showed that the EIS only contains a single time constant. Moreover, the maximum value of phase angle is lower than 90°, which may be due to a deviation from the ideal capacitor behavior [23]. This phenomenon is caused by the in-homogeneity of the surface film layer [24]. Therefore, a constant phase element Q is used here.

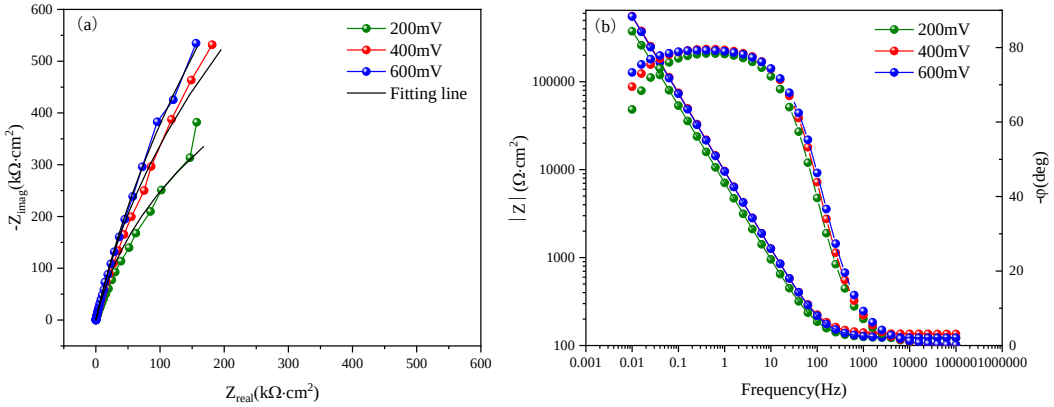

Figure 3. Nyquist plots of AISI321 stainless steels in 36% ethylene glycol-water solution: (a) Nyquist plots and (b) Bode plots.

The equivalent circuit shown in Fig. 4 is used to analysis the EIS data. In Figure 4, R_s and R_t are representative of the solution resistance and charge-transfer resistance, respectively. Q is associated with the capacitance behavior of the film [13], and the R_t can reflect the protection performance of the passive film. Relevant fitting parameters of equivalent circuit are shown in Table 3. It is clear that the value of R_t increases with the increasing passivation potential, from 1330 Ω·cm^2 to 4800 Ω·cm^2 as the passivation potential increases from 200 to 600 mV, indicating that the passive film formed at high potential provides a much better protection performance.

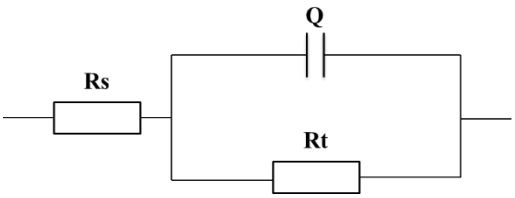

Figure 4. Equivalent circuit *R(QR)* of EIS

Table 3 Fitted results of the EIS with the equivalent circuit.

Fitting parameters	200 mV	400 mV	600 mV
R_s (Ω·cm^2)	121.6	135.4	122.2
Q (μF·cm^2·s^{n-1})	27.93	20.14	20.56
n	0.8832	0.8927	0.8870
R_t (kΩ·cm^2)	1330	2929	4800

3.3. Mott-Schottky tests

The Mott-Schottky curves of various passive films formed on the surface of AISI321 in the ethylene glycol-water solution at 200, 400 and 600 mV are shown in Fig. 5(a). An examination of the plots indicates that the passive films display n-type semiconductor feature in the range from -0.15 to

0.45 V, as shown in the positive slope, while the passive films present p-type semiconductor characteristic in the potential range from 0.45 to 0.75 *V*, as shown in the negative slope plots.

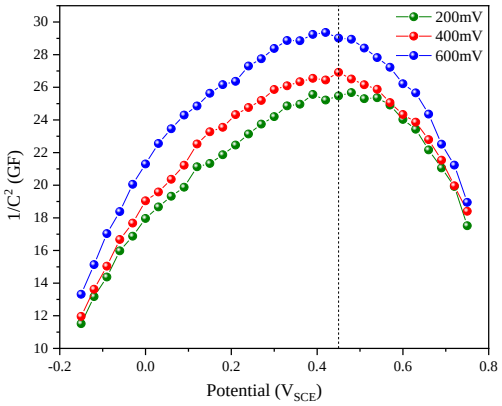

Figure 5. Mott–Schottky plots of the passive films formed at different potentials after 4 h in 36% ethylene glycol-water solution.

Based on the Mott-Schottky theory [25], the capacitances of space charge of the n-type and p-type semiconductors are given by Equations (1) and (2), respectively

where ε_0 is the vacuum permittivity (8.854×10^{-12} F·m^{-1}), ε represents the dielectric constant of the film (ε=12) [26, 27], k represents the Boltzmann constant (1.38×10^{-23} J·K^{-1}), e represents the electron charge (1.6×10^{-19} C), N_D and N_A are the donor and acceptor densities, respectively, T is the absolute temperature and E_{fb} is the flat-band potential. For the p-type semiconductor, the slope of Mott–Schottky plots should be negative, while the n-type semiconductor exhibits a positive slope.

Table 4. Carrier density of the oxide layers formed at various potential values.

Film formation Potential (mV_{SCE})	Carrier density (10^{20}·cm^{-3})		
	N_D	N_A	N_D+ N_A
200	3.62	3.71	7.33
400	3.14	3.69	6.83
600	3.02	3.07	6.09

The densities of donor and acceptor can be calculated by fitting Eqs. (1) and (2). The results are shown in Table 4. The donor density is approximately 10^{20} cm^{-3} for all of the experiments. A stable oxide layer has not yet formed on the the sample surface when potential is lower so the N_D and N_A value are larger at lower potential. In addition, the carrier density is low at higher passive film formation potential because a stable and compact passive film appeared on the surface. According to the point defect model

[28], part of the ions can be absorbed by oxygen vacancies, which may result in a decrease of protection effect of the passive film. Therefore, when formed at potential 200 mV, the density of the carrier is higher than that at 400 and 600 mV, demonstrating that the passive film formed at 200 mV contains a larger defect concentration and has lower corrosion resistance.

3.4. Surface morphology of passive films

The in situ EC-AFM topography images at three different potentials for 60 min are shown in Fig. 6. And the diameter of the particles increased with increasing passivation potential from 0.2 to 0.4 V and 0.6 V.

Figs. 6(a_1), 6(a_2) and 6(a_3) show the AFM topographic images of the steel specimens polarized at -0.2 V_{SCE} in the solution for 10 min, 30 min and 60 min, respectively. A few grooves form on the surface of the sample after 10 min of passivation. As the passivating time increase to 30 min and 60 min, the grooves connect together, and the film becomes complete

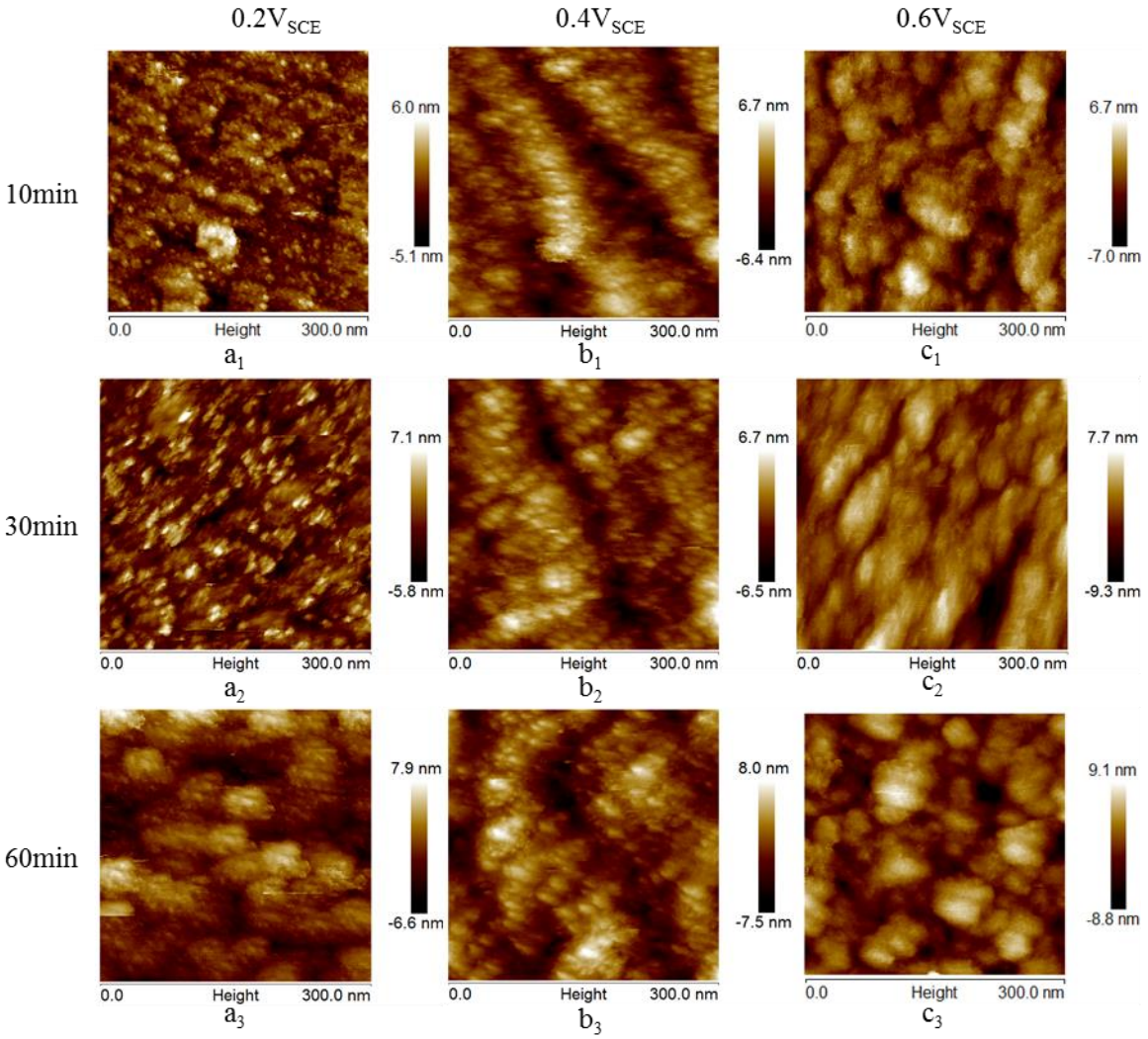

Figure 6. AFM images of the film structure on AISI321 stainless steels at different potentials for 1 h in the 36% ethylene glycol-water solution.

Figs. 6(b_1), 6(b_2) and 6(b_3) show the AFM topographic images of the steel specimens polarized at 0.4 V_{SCE} in the solution for 10 min, 30 min and 60 min, respectively. The grooves generated by the surface finishing on the specimen are clearly visible in the image obtained after 10 min of passivation, suggesting that a complete film is not formed on the surface. After 30 min of passivation, the film is more clear. Additionally, the morphology is similar to that of the sample polarized at 0.2 V_{SCE} for 60 min. As the passivating time increases to 60 min, the diameter of the particles increases, indicating the growth of the passive film on the steel surface, as shown in Fig. 6(b_3).

Figs. 6(c_1), 6(c_2) and 6(c_3) show the AFM images of the steel specimen polarized in the solution at 0.6 V_{SCE} for 10 min, 30 min and 60 min, respectively. After 10 min of polarization, numerous nanoscale particles with the diameter of approximately 30 nm are distributed on the specimen surface, as observed in Fig. 6(c_1). When the polarization time increases to 30 min, a whole film is formed on the surface, as observed in Fig. 6(c_2). After 60 min of passivation, the size of the particles increases further.

3.5. XPS analysis

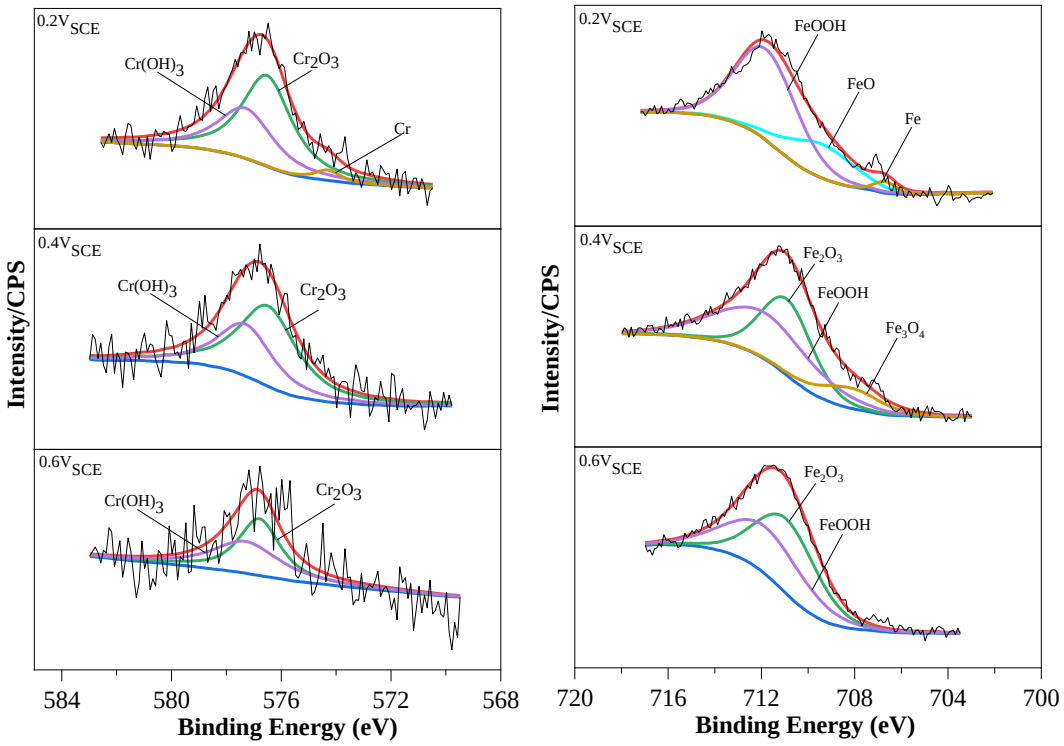

Figure 7. XPS survey spectrum of (a) Cr $2p_{3/2}$ and (b) Fe $2p_{3/2}$ of the passive films formed on AISI321 stainless steels after being passive at various potentials for 4 h in the 36% ethylene glycol-water solution.

XPS tests were implemented to further investigate the composition of the passive filmsat various applied potentials for 4 h in the ethylene glycol-water solution. As shown in Fig. 7, the results are divided into contributions of the different oxidation state. The main compounds of the passive film regarding chromium and iron are analyzed based on the binding energies (E_b), as shown in Table 5 [32].

For the passive film formed at 200 mV, the fitted results show that the Cr $2p_{3/2}$ spectrum is divided

into three peaks at 574.3 eV, 577.3 eV and 576.8 eV, corresponding to Cr, $Cr(OH)_3$ and Cr_2O_3, respectively. The value of the $Cr(OH)_3$ and Cr_2O_3 intensities are obviously higher than that of the Cr(met). The main constituents of the passive film are metal oxides. The spectra of Fe $2p_{3/2}$ can be divided into three primary peaks including the metallic state, the FeO and FeOOH.

The Cr $2p_{3/2}$ spectra at 400 mV for 4 h shows that the passive film is mainly composed of $Cr(OH)_3$ and Cr_2O_3. The concentration of the Cr (met) decreases, however the Cr_2O_3 concentration increases with the increasing of potential. The Fe $2p_{3/2}$ spectra can be divided into three primary peaks, which represent the Fe_2O_3, the Fe_3O_4 and FeOOH, respectively. The corresponding peak heights of Fe_3O_4 and Fe_2O_3 indicate that the passive film at 400 mV mainly consists of the iron oxide species.

The spectra for 600 mV in the solution are also shown in Fig. 7. None of Fe_3O_4 and FeO peaks are obtained according to the fitting results. And it is can be clearly observed that the main composition of the passive film are Fe_2O_3 and FeOOH. The Cr $2p_{3/2}$ spectra have two various peaks, representing $Cr(OH)_3$ and Cr_2O_3. The concentration of the Cr_2O_3 in the passive film increases comparing with that formed at lower potential.

Table 5. Binding energies of the primary compounds of the passive film in Figure 7.

Peak	Species and binding energy (eV)
Fe $2p_{3/2}$	Fe(met) 706.7; Fe_3O_4 708.2; FeO 709.4; Fe_2O_3 710.9; FeOOH/711.8
Cr $2p_{3/2}$	Cr(met) 574.3; Cr_2O_3 576.8; $Cr(OH)_3$ 577.3

4. CONCLUSIONS

(1) The AISI321 stainless steel can be passivated in the ethylene glycol-water solution over a wide passive potential range from -0.15 to 0.75 V. As the passive potential increases, the protection performance of the passive film increases significantly.

(2) Mott-Schottky tests reveal that the specimen exhibits n-type and p-type properties alternately at different applied potential ranges. When the potential is between -0.15 and 0.45 V, n-type oxide films are most likely formed on the surface. At the potential range from 0.45 to 0.75 V, p-type oxide films adhere to the surface of the sample as oxide films. The passive film formed at high potential contains a much lower concentration of defects and provides better protection performance.

(3) According to the EC-AFM results, the passive film becomes more complete, and the amount of the defects decreases with increasing polarization time. In addition, the passive film formed at higher potential has much lower concentration of defects and provides better protection performance.

ACKNOWLEDGEMENT
This work was supported by the National Natural Science Foundation of China (No. 51471033), the National Basic Research Program of China (973 Program, No. 2014CB643300), and the National Environment Corrosion Platform (NECP).

References

1. N. Baddoo, *Struct. Eng.*, 91 (2013) 10.
2. X. Cheng, Z. Feng, C. Li, C. Dong and X. Li, *Electrochim. Acta*, 56 (2011) 5860.
3. L. Gardner, Prog. *Struct. Eng. Mater.*, 7 (2005) 45.
4. H. Luo, C.F. Dong, K. Xiao and X.G. Li, *Appl. Surf. Sci.*, 258 (2011) 631.
5. O.K. Abiola and J.O.E. Otaigbe, *Corros. Sci.*, 50 (2008) 242.
6. G.A. Zhang, L.Y. Xu and Y.F. Cheng, *Electrochim. Acta*, 53 (2008) 8245.
7. M. Niknejad Khomami, I. Danaee, A.A. Attar and M. Peykari, *Trans. Indian. Inst. Met.*, 65 (2012) 303.
8. I. Danaee, M. Niknejad Khomami and A.A. Attar, *J. Mater. Sci. Technol.*, 29 (2013) 89.
9. M. Niknejad Khomami, I. Danaee, A.A. Attar and M. PeykariMet, *Mater. Int.*, 19 (2013) 453.
10. I. Danaee, M. Niknejad Khomami, *Mat.-wiss. u.Werkstofftech*., 11 (2012) 43.
11. I. Danaee, M. Niknejad Khomami, and A.A. Attar, *Mater. Chem. and Phys.*, 135 (2012) 658.
12. X. Chen, W. Tian and S. Li, *Chinese J. Aeronaut.*, 29 (2016) 1142.
13. Z. Feng, X. Cheng, C. Dong, L. Xu and X. Li, *Corros. Sci.*, 52 (2010) 3646.
14. M.F. Montemor, M.G.S. Ferreira, N.E. Hakiki and M. Da Cunha Belo, *Corros. Sci.*, 42 (2000) 1635.
15. I. Nicic, D.D. Macdonald, *J. Nucl. Mater.*, 379 (2008) 54.
16. A. Fattah-alhosseini, M.A. Golozar, A. Saatchi, *Corros. Sci.*, 52 (2010) 205.
17. S.F. Yang, D.D. Macdonald, *Electrochim. Acta*, 52 (2007) 1871.
18. P. Yi, C. Dong, K. Xiao, C. Man and X. Li, J. *Electroanal. Chem.*, 809 (2018) 52.
19. M. Urquidi-Macdonald, S. Real, D.D. Macdonald, *J. Electrochem. Soc.,* 133 (1986) 2018.
20. H. Shin, F. Mansfeld, *Corros. Sci.*, 28 (1988) 933.
21. M. Urquidi-Macdonald, S. Real, D.D. Macdonald, *Electrochim. Acta*, 35 (1990) 1559.
22. M.S. Akram, V. Lomadze, *Systems Control Lett.*, 58 (2009) 83.
23. J. Lv, T. Liang, C. Wang, *Energy*, 112 (2016) 67.
24. M.V. Cardoso, S.T. Amaral, E.M.A. Martini, *Corros. Sci.*, 50 (2008) 2429.
25. A.D. Paola, *Electrochim. Acta*, 34 (1989) 203.
26. F. Gaben, B. Vuillemin and R. Oltra, *J. Electrochem. Soc.*, 151 (2004) B595.
27. G. Goodlet, S. Faty, S. Cardoso, P.P. Freitas, A.M.P. Simoes and M.G.S. Ferreira, *Corros. Sci.*, 46 (2004) 1479.
28. D.D. Macdonald, *J. Electrochem. Soc.*, 139 (1992) 3434.
29. D.D. Macdonald, *J. Electrochem. Soc.*, 153 (2006) B213.
30. E. Sikora, J. Sikora, and D.D. Macdonald, *Electrochim. Acta*, 41 (1996) 783.
31. A. Xu, C. Dong, X. Wei, F. Mao, X. Li and D.D. Macdonald, *Electrochem. Commun.*, 68 (2016) 62.
32. J.F. Moulder, F.S. William and E.S. Peter, Handbook of X-ray Photoelectron Spectroscopy, Perkin-Elmer Corporation, (1992), USA.